JCI insight

RESEARCH ARTICLE

Chemical inhibition of FBXO7 reduces inflammation and confers neuroprotection by stabilizing the mitochondrial kinase PINK1

Yuan Liu,[1,2] Travis B. Lear,[1,3] Manish Verma,[4] Kent Z.Q. Wang,[4] P. Anthony Otero,[4] Alison C. McKelvey,[1] Sarah R. Dunn,[1] Erin Steer,[4] Nicholas W. Bateman,[5] Christine Wu,[5] Yu Jiang,[6] Nathaniel M. Weathington,[1] Mauricio Rojas,[1] Charleen T. Chu,[2,4,7,8] Bill B. Chen,[1,9] and Rama K. Mallampalli[1,5,10]

[1]Department of Medicine, the Acute Lung Injury Center of Excellence, [2]The McGowan Institute for Regenerative Medicine, [3]Department of Environmental and Occupational Health, Graduate School of Public Health, and [4]Department of Pathology, University of Pittsburgh School of Medicine, Pittsburgh, Pennsylvania, USA. [5]Department of Cell Biology and [6]Department of Pharmacology and Chemical Biology, University of Pittsburgh, Pittsburgh, Pennsylvania, USA. [7]Department of Ophthalmology, [8]The Pittsburgh Institute for Neurodegenerative Diseases, [9]Vascular Medicine Institute, and [10]Medical Specialty Service Line, Veterans Affairs Pittsburgh Healthcare System, Pittsburgh, Pennsylvania, USA.

Mitochondrial quality control is mediated by the PTEN-induced kinase 1 (PINK1), a cytoprotective protein that is dysregulated in inflammatory lung injury and neurodegenerative diseases. Here, we show that a ubiquitin E3 ligase receptor component, FBXO7, targets PINK1 for its cellular disposal. FBXO7, by mediating PINK1 ubiquitylation and degradation, was sufficient to induce mitochondrial injury and inflammation in experimental pneumonia. A computational simulation–based screen led to the identification of a small molecule, BC1464, which abrogated FBXO7 and PINK1 association, leading to increased cellular PINK1 concentrations and activities, and limiting mitochondrial damage. BC1464 exerted antiinflammatory activity in human tissue explants and murine lung inflammation models. Furthermore, BC1464 conferred neuroprotection in primary cortical neurons, human neuroblastoma cells, and patient-derived cells in several culture models of Parkinson's disease. The data highlight a unique opportunity to use small molecule antagonists that disrupt PINK1 interaction with the ubiquitin apparatus to enhance mitochondrial quality, limit inflammatory injury, and maintain neuronal viability.

Authorship note: CTC, BBC, and RKM contributed equally to this work.

Conflict of interest: A patent application (PCT/US2018/039327) relating to this study was submitted jointly by the US Department of Veterans Affairs and the University of Pittsburgh on behalf of YL, CTC, BBC, and RKM.

Submitted: July 16, 2019
Accepted: April 23, 2020
Published: June 4, 2020.

Reference information: *JCI Insight*. 2020;5(11):e131834. https://doi.org/10.1172/jci.insight.131834.

Introduction

PTEN-induced kinase 1 (PINK1), a serine/threonine protein kinase, functions in a critical role for mitochondria quality maintenance (1, 2). Loss-of-function mutations in the *PINK1* gene cause mitochondrial dysfunction and an early-onset familial form of Parkinson's disease (3–5). PINK1 contains an NH_2-terminal mitochondrial–targeting sequence (6) that facilitates its entry into mitochondria to modulate the lifespan of mitochondrial respiratory chain subunits (7). PINK1 can accumulate on the outer mitochondrial membrane after cell stress to recruit parkin (a ubiquitin E3 ligase) to regulate mitochondrial disposal by mitophagy (8). Parkin, mitochondrial protease HtrA2, mitochondrial chaperone TRAP1, Akt, and protein kinase A are known molecular targets described for PINK1 (9–13). Collectively, these observations suggest multiple mechanisms whereby PINK1 can regulate mitochondrial and cytosolic substrates that, in turn, impact cellular bioenergetics and human disease.

In the brain, PINK1 has shown diverse cytoprotective effects. Cellular depletion of PINK1 triggers neuronal cell death, possibly through complex interactions with several client proteins including Akt (14). *PINK1* deficiency also leads to reduced dopamine levels, essential for coordinated motor function, and triggers synaptodendritic shrinkage (13, 15, 16) and the release of inflammatory cytokines such as TNF-α, IL-1β, and COX-2 by astrocytes and microglia, and after injury in the brain (17–19). These observations suggest that approaches that maintain or increase cellular PINK1 protein concentrations may provide important opportunities to preserve chemical energy stores during aging or stress and to

limit neurodegeneration, cell death, and inflammation. In this regard, PINK1 undergoes limited proteolysis, and the cleaved PINK1 fragment is degraded by the ubiquitin proteasome system (UPS) (20). Here, we show that the PINK1 protein is targeted for its cellular elimination by the ubiquitin E3 ligase subunit, FBXO7. We identified a compound that attenuates FBXO7 and PINK1 interaction, retains mitochondrial integrity, and confers cytoprotection in several complementary models.

Results

As the UPS may show selectivity for different forms of a given protein target (21), we investigated whether or not full-length PINK1 is subjected to ubiquitin-mediated degradation by evaluating the ability of proteasomal or lysosomal inhibitors to regulate stability of the kinase. Considering the well-recognized difficulty in detecting endogenous PINK1 protein, we used human BEAS-2B cells that are rich in mitochondria to observe that both full-length and a fragment of PINK1 undergo rapid degradation when protein synthesis is blocked by the addition of the protein biosynthesis inhibitor cycloheximide (CHX) (Figure 1A). Moreover, addition of the proteasome inhibitor MG132 accumulated not only the PINK1 fragment, but also full-length PINK1, while the lysosomal inhibitor leupeptin had little impact on basal PINK1 turnover. To further explore if PINK1 is subject to ubiquitin-dependent degradation, we constructed a series of V5-tagged lysine to arginine (K–R) mutants that were expressed in cells to measure exogenous PINK1 protein turnover, as shown in Supplemental Figure 1, A and B (supplemental material available online with this article; https://doi.org/10.1172/jci.insight.131834DS1). The triple mutations of 3 highly exposed, juxtaposed lysine sites (K520, K523, and K526) in PINK1 resulted in an optimally extended half-life ($t_{½}$), compared with WT PINK1 (Supplemental Figure 1C). These findings confirmed that full-length PINK1 protein is also subjected to ubiquitin-proteasome mediated degradation likely through multisite ubiquitylation. Ubiquitin tagging to a target protein is orchestrated by an enzymatic cascade involving highly conserved E1, E2, and a specific ubiquitin E3 ligase (22). F-box proteins recognize and recruit substrates to a ubiquitin E3 ligase catalytic core (Skp1-Cul1-Rbx1) for ubiquitylation and subsequent degradation (23, 24). To identify the ubiquitin E3 ligase that tags PINK1 for proteasomal disposal, we used PINK1 as bait for IP–mass spectrometry and identified the F-box protein FBXO7 as a PINK1 binding partner (Supplemental Table 1). FBXO7 partakes in mitophagy in response to mitochondrial damage (25, 26), and mutations in the *FBXO7* gene have been identified in families with Parkinson's (27, 28). We overexpressed *FBXO7* and detected decreased PINK1 protein levels with increasing amounts of *FBXO7* plasmid expression (Figure 1B). *FBXO7* knockdown confirmed that decreased FBXO7 led to accumulation of endogenous PINK1 protein and extends PINK1 lifespan ($t_{½}$) in cells (Figure 1, C and D). Additionally, in vitro ubiquitylation assays confirmed that FBXO7 enhances PINK1 polyubiquitylation (Figure 1E). These data suggest that FBXO7 mediates PINK1 polyubiquitylation and proteasomal degradation.

We next examined the role of FBXO7 on mitochondrial homeostasis, given the important role played by PINK1 in regulating mitochondrial function. We monitored mitochondrial membrane potential ($\Delta\Psi$) in *FBXO7*-overexpressed cells using a $\Delta\Psi$-dependent dye JC1. In depolarized mitochondria, JC1 experiences a fluorescence shift from red to green. Using the mitochondria depolarizer carbonyl cyanide m-chlorophenylhydrazone (CCCP) as a positive control, we found that overexpression of *FBXO7* impairs the $\Delta\Psi$ (Figure 2A), indicated by the decrease of fluorescence ratio of red/green, which is similar to effects previously reported in PINK1-KO neurons and cells (29). We then employed a different $\Delta\Psi$ dye, MitoSense Red, combined with flow cytometry to evaluate mitochondrial damage in *FBXO7*-overexpressed cells. Compared with cells transfected with control plasmid, overexpression of *FBXO7* increased the content of depolarized mitochondria from 16.1%–33.6% (Figure 2B), determined by a red fluorescence decrease. *FBXO7* overexpression with CCCP treatment increased numbers of damaged mitochondria from 25.5%–38% compared with CCCP alone, suggesting that FBXO7 exerts an additive effect on mitochondrial injury induced by CCCP. Conversely, *FBXO7* knockdown largely protected mitochondria from CCCP-induced injury (Figure 2C).

Given the newly described antiinflammatory role of PINK1 in the lung (19, 30) and its identification here as a substrate for FBXO7-mediated degradation, we examined effects of FBXO7 on mitochondria and lung inflammation. First, we observed that the gram-negative bacterial component, LPS increased FBXO7 mass and decreased PINK1 protein levels in lung epithelia (data not shown). Likewise, a virulent strain of the gram-negative pathogen, *P. aeruginosa* (PA103), resulted in reduced $\Delta\Psi$ (Supplemental Figure 2A) and the appearance of swollen mitochondria with disrupted cristae (Supplemental Figure 2B). Mice infected with empty lentivirus or lentivirus encoding *FBXO7* were subsequently challenged with PA103.

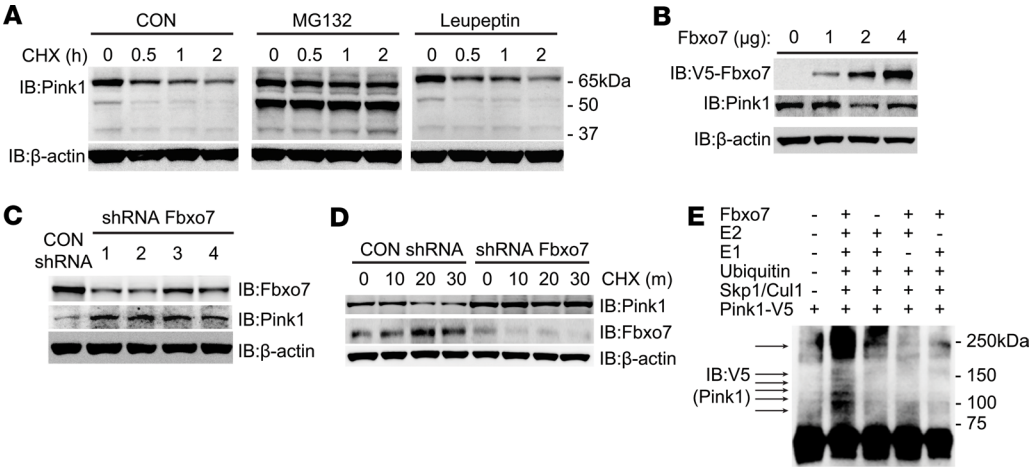

Figure 1. Fbxo7 mediates PINK1 ubiquitination and degradation. (**A**) BEAS-2B cells were pretreated with MG132 (20 μM), leupeptin (100 μM), or DMSO (control, CON) for 30 minutes, and then CHX (40 μg/mL) was added to assay protein decay. (**B**) BEAS-2B cells were nucleofected with V5-tagged *Fbxo7* plasmid at indicated amounts and incubated for 48 hours before immunoblotting. (**C**) BEAS-2B cells were nucleofected with 4 individual shRNAs separately and incubated for 72 hours before immunoblotting. (**D**) BEAS-2B cells were nucleofected with control shRNA or *Fbxo7* shRNA for 72 hours and then treated with CHX (40 μg/mL) for half-life analysis. (**E**) In vitro ubiquitylation assays were performed with synthesized PINK1 combined with indicated recombinant proteins.

Compared with an empty lentivirus control group, i.t. introduction of *FBXO7* significantly increased bronchoalveolar lavage (BAL) protein concentration, lavage cell counts, and cell infiltrates (Figure 3, A, B, and G). *FBXO7* overexpression also increased the release of proinflammatory cytokines TNF-α, IL-1β, and IL-6 in the lung (Figure 3, D–F). PA103 infection combined with *FBXO7* overexpression in the lung further accentuated lung inflammatory injury, indicated by increased lavage protein concentration, cell counts, cytokines, and cell infiltrates, compared with the control group or each component administered individually. However, overexpressed *FBXO7* did not alter the lavage bacterial load (Figure 3C). In mouse lung tissue, PA103 infection induced endogenous FBXO7 protein levels compared with control, with a corresponding reduction in PINK1 content (Figure 3H). Compared with the *FBXO7*-overexpression group, additional PA103 infection further augmented this reduction of PINK1 protein levels. These data as a whole indicate that *FBXO7* pulmonary gene transfer is sufficient to trigger tissue inflammatory injury, a process that is further accentuated with concomitant PA103 infection.

In contrast, *FBXO7* shRNA decreased BAL protein concentration and cell counts without altering bacterial counts in PA103-infected mice (Figure 4, A–C). Additionally, *FBXO7* knockdown attenuated the release of proinflammatory cytokines and exhibited histological evidence of reduced tissue cell infiltrates (Figure 4, D–G). Immunoblotting data from lungs confirmed that *FBXO7* knockdown restored PINK1 protein levels, despite bacterial infection (Figure 4H). Thus, FBXO7 functions as a proinflammatory protein in vivo by downregulating the PINK1 antiinflammatory axis, suggesting that FBXO7 may serve as a potential pharmacologic target.

We analyzed the FBXO7 structure, focusing on the Fbxo7/PI31 domain (FP domain) within its C-terminus, which is crucial for its interaction with substrates or regulatory proteins (31). We hypothesized that small molecule inhibition of the FP domain will induce a conformational change, thereby disrupting the ability of FBXO7 to capture PINK1. We utilized FP domain crystal structure (PDB structure 4L9C.pdb) (Figure 5A). Using molecular docking analysis and score-ranking operations on the FBXO7-FP domain 3-D structure model, we assessed potential ligands that might fit the FP domain cavities. These docking experiments were conducted using the LibDock program from Discovery Studio 3.5. A library containing 3 million small molecule compounds was first used to screen potential ligands for the FBXO7-FP domain. In this model, GLN215, LYS227, LYS235, SER247, and LYS266 residues within the FP domain are important for interacting with inhibitors (Figure 5A). The top 20 score-ranking molecules were selected and further evaluated using in vitro experiments. We then tested if 1 selected compound, BC1464, that engages FBXO7 affected the interaction between FBXO7 and PINK1. In vitro binding assays demonstrated that increasing amounts of BC1464 efficiently decreased the interaction between FBXO7 and PINK1 (Figure 5B). BC1464 also increased PINK1 protein levels in cells in a

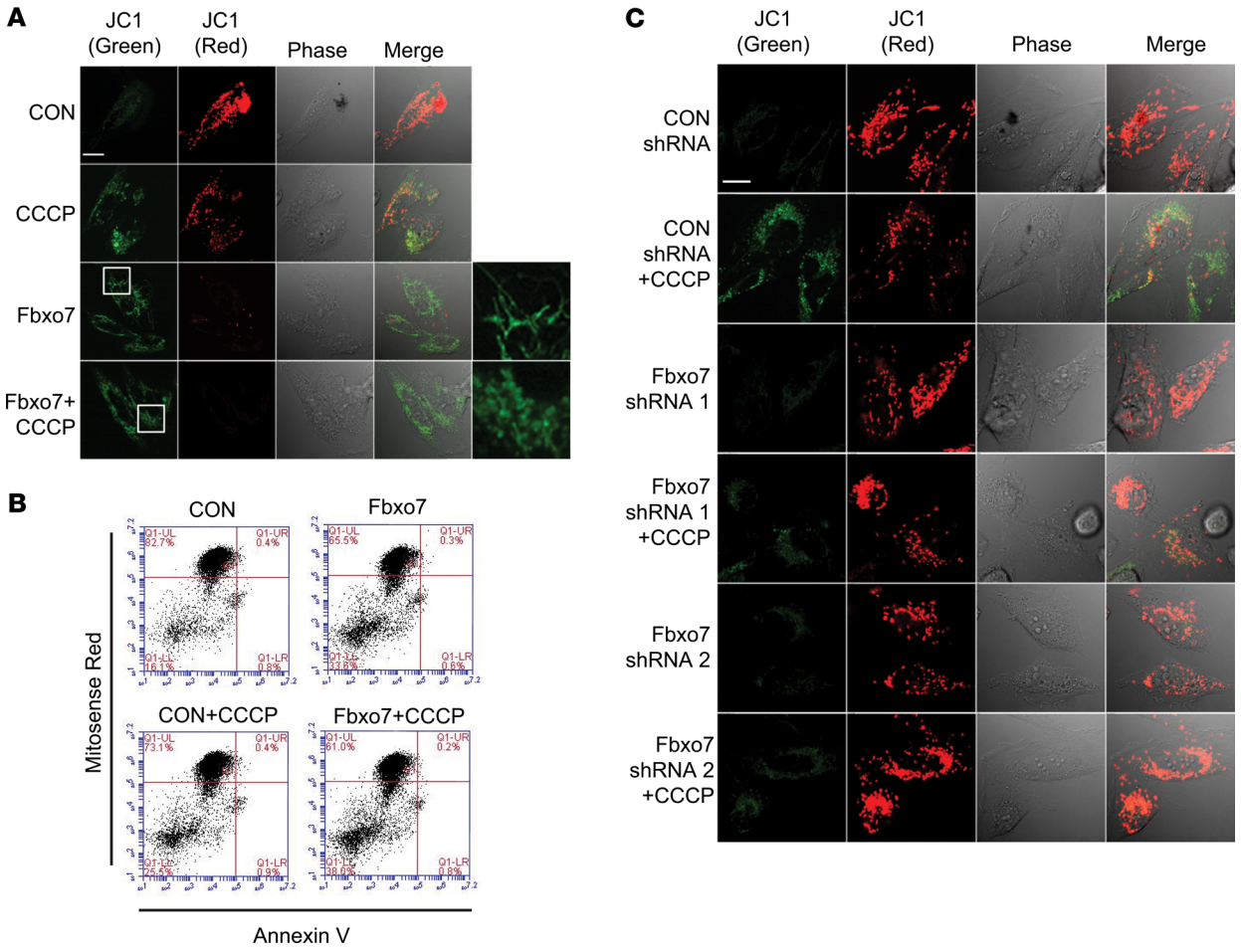

Figure 2. Fbxo7 triggers mitochondrial injury. (**A** and **C**) BEAS-2B cells were nucleofected with control or *Fbxo7* plasmid for 48 hours or shRNAs for 72 hours. Cells were treated with 50 μM CCCP for 5 minutes where indicated, and then stained with JC1 (2 μM) for additional 20 minutes for confocal microscopic analysis. Scale bars: 10 μm. (**B**) BEAS-2B cells were nucleofected with control or *Fbxo7* plasmid for 48 hours and then were treated with or without CCCP (20 μM) for 1 hour. The cells were stained with MitoSense Red and annexin V for flow cytometry analysis.

dose-dependent manner (Figure 5C). This was not seen using a control compound BC1465, which shares the same quinazoline core with different side chain structures unfit for the FBXO7 cavity. Endogenous full-length PINK1 rapidly degrades upon inhibiting protein synthesis; however, addition of BC1464 largely stabilized PINK1, while compound BC1465 showed no effect on PINK1 protein stability (Figure 5D). Neither BC1464 nor the control compound, BC1465, affected the mRNA levels of PINK1 or of FBXO7 (Supplemental Figure 3A). The addition of BC1464 elicited a dose-dependent increase in PINK1 levels in control cells with normal levels of FBXO7, while knockdown of *FBXO7* caused a basal increase of PINK1 (Figure 5E). Notably, no further PINK1 protein increase was observed with addition of BC1464 to FBXO7-deficient cells (Figure 5E), suggesting that BC1464 elevates PINK1 protein levels through inhibiting FBXO7.

We next examined if small molecule inhibition of FBXO7 modulates mitochondrial function. BC1464 prevented CCCP-triggered mitochondrial injury as assessed using MitoSense Red and annexin V staining, decreasing the numbers of CCCP-damaged mitochondria from 17.2%–10.5% (Figure 6, A and B). In rat myoblast H9C2 cells, rich in mitochondria, JC1 staining demonstrated that BC1464 maintains the $\Delta\Psi$ damaged by CCCP, compared with the control vehicle and BC1465 groups (Figure 6C). These data suggest that the FBXO7 inhibitor preserves PINK1 levels and supports the maintenance of mitochondrial function after depolarizing stress. In human PBMCs, the LPS-stimulated release of the proinflammatory cytokine TNF-α was reduced by about 37% at 1 ng/mL and potently blocked at 10 ng/mL of BC1464 (Supplemental Figure 3B). BC1464 also selectively increased PINK1 protein levels and inhibited proinflammatory TNF-α release in response to endotoxin in human lung explants (Supplemental Figure 3, C and D). These results indicate that small molecule inhibition of the interaction between FBXO7 and PINK1 reduces inflammation in human cells.

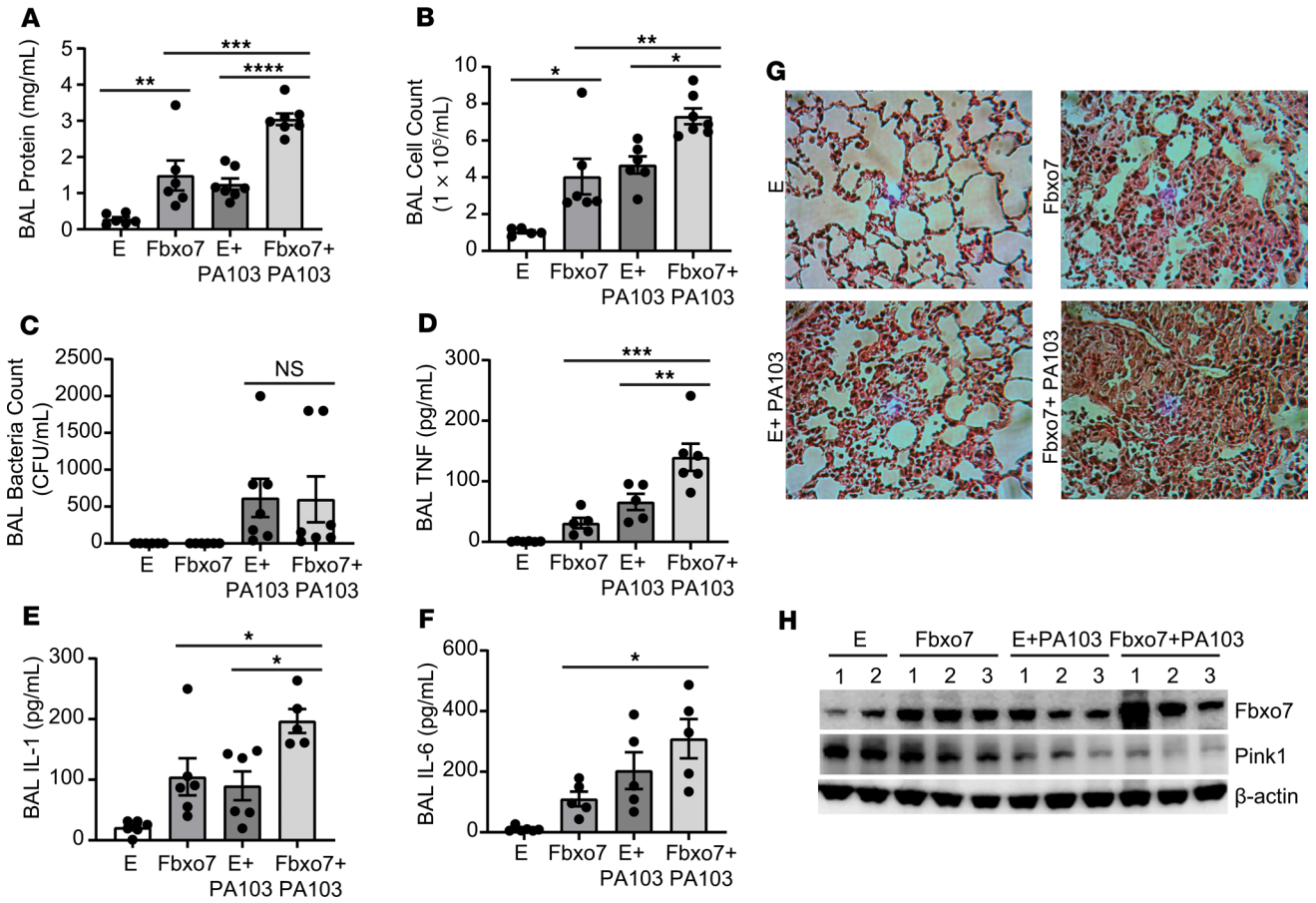

Figure 3. Fbxo7 induces experimental lung inflammation with loss of PINK1. C57BL/6N mice were administered i.t. with Lenti-control or Lenti-Fbxo7 (1×10^8 PFU/mouse) for 144 hours, and 5–6 mice/group were then inoculated with PA103 (1×10^4 PFU/mouse) for 18 hours. Mice were euthanized, and lungs were lavaged with saline, harvested, and then homogenized. (**A–F**) Bronchoalveolar lavage protein, cell count, bacteria loads, and cytokine secretion were measured in. (**G**) H&E staining was performed on lung samples; original magnification, 100×. Data are shown as means ± SEM of 5–6 mice/group. (**H**) Randomly chosen mouse lung tissue from each group was homogenized and subjected to immunoblotting analysis. $^*P < 0.05$, $^{**}P < 0.01$, $^{***}P < 0.001$, $^{****}P < 0.0001$, as indicated by 1-way ANOVA with Tukey's test of multiple comparisons (**A–F**).

We next tested the FBXO7 inhibitor in experimental mouse pneumonia in which mitochondrial injury plays a vital role. Consistent with our previous observations, PA103 infection potently triggered lung inflammatory injury (Figure 7, A, B, and G). BC1464 had no effect on lavage bacteria counts (Figure 7C). However, compared with control groups, administration of BC1464 significantly decreased lavage protein, cell numbers, cytokine levels, and tissue infiltrates with restoration of PINK1 levels (Figure 7, A, B, and D–H).

As PINK1 mutations are linked to neurodegenerative disorders such as Parkinson's disease, we tested BC1464 in several Parkinson's disease models. First, we established that human SH-SY5Y neuroblastoma cells stably express FBXO7, and that BC1464 stabilizes PINK1 expression in the presence of CHX in neuronal cells with an IC_{50} of 5.2 μg/mL (Figure 8, A and B). We studied the efficacy of BC1464 in disrupting the FBXO7/PINK1 interaction in PINK1-FLAG–tagged SH-SY5Y cells using proximity ligation assay (PLA). This technique involves immunostaining for the interaction targets using secondary antibodies tagged with oligonucleotide sequences that serve as primers for rolling circle amplification. Amplification only occurs when the antibody targets are in close proximity, and the products are quantified fluorescently. Using this assay, we established a strong PLA signal for FBXO7 and PINK1-FLAG indicative of their interaction. BC1464 elicited significant, dose-related decreases in the PLA signal relative to vehicle (Figure 8, C and D).

PINK1 is known to phosphorylate ubiquitin (32) and the catalytic subunit of protein kinase A (PKAc) (13). To determine whether or not BC1464 increased these markers of PINK1 activity in living cells, we performed Western blot analysis for phosphorylated ubiquitin and phosphorylated PKAc in SH-SY5Y cells treated with vehicle, BC1464, or BC1465. We found that BC1464 increased

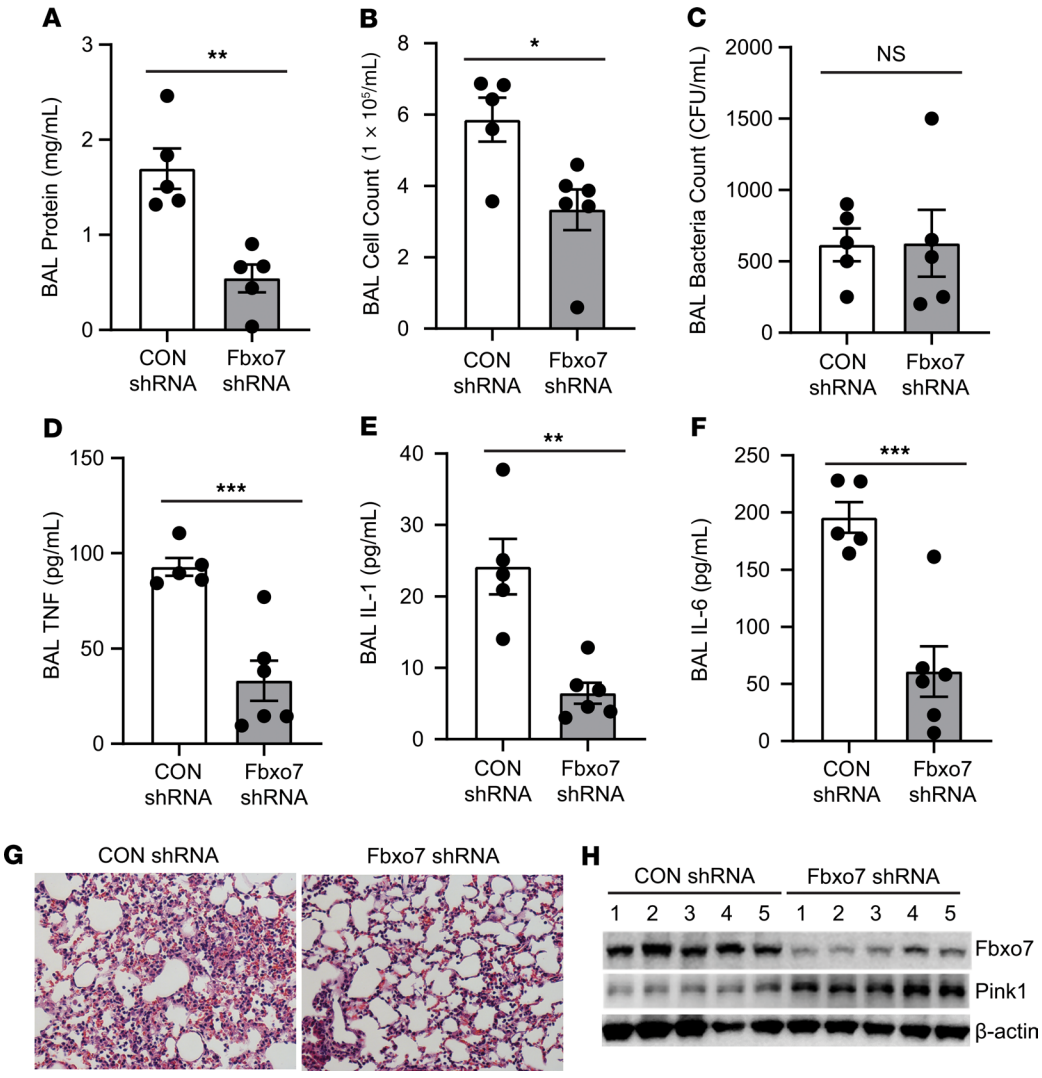

Figure 4. Fbxo7 knockdown attenuates bacterial-induced lung inflammation. C57BL/6N mice were administered i.t. with Lenti-control shRNA or Lenti-Fbxo7 shRNA (1×10^8 PFU/mouse) for 144 hours. Mice were then euthanized, and lungs were lavaged with saline, harvested, and then homogenized. (**A–F**) Lavage protein, cell count, bacteria loads, and cytokine secretion were measured. (**G**) H&E staining was performed on lung samples; original magnification, 100×. Data are shown as means ± SEM of 5–6 mice/group. (**H**) Mouse lung tissue from each group was homogenized and subjected to immunoblotting analysis. $^*P < 0.05$, $^{**}P < 0.01$, $^{***}P < 0.001$, relative to CON shRNA by 2-tailed Student's *t* test (**A–F**).

immunoreactivity to phospho-ubiquitin and phospho-PKAc (Figure 8, E–G), suggesting an ability to activate mitochondrial and cytosolic PINK1 signaling pathways within cells.

Having established that BC1464 disrupts the FBXO7 and PINK1 interaction in neuroblastoma cells, eliciting increased PINK1 expression and function, we studied the effects of BC1464 on neuronal cell injury induced by the complex I inhibitor 1-methyl-4-phenylpyridinium (MPP+). Parkinson's disease is characterized by reduced complex I activity, and MPP+ — the active metabolite of 1-methyl-4-phenyl-1,2,3,6-tetrahydropyridine (MPTP) that causes a human Parkinsonian syndrome — is frequently used to model Parkinsonian cell death (33–35). Elevated PINK1 is known to protect against MPTP/MPP+ toxicity (36). Similarly, we found that BC1464 significantly decreased MPP+-elicited injury in human SH-SY5Y cells relative to the inactive control BC1465 (Figure 8H). Likewise, in primary cortical neurons, the interaction inhibitor BC1464 protected against the cytotoxic effects of MPP+ (Figure 8I).

Neurodegeneration is characterized by neurite retraction, a phenotype that is not generally reversed even if cell death is arrested (37). Given that PINK1 plays a key role in rescuing dendrite complexity (13), we examined the effects of BC1464 versus BC1465 on dendritic injury in primary cortical neurons.

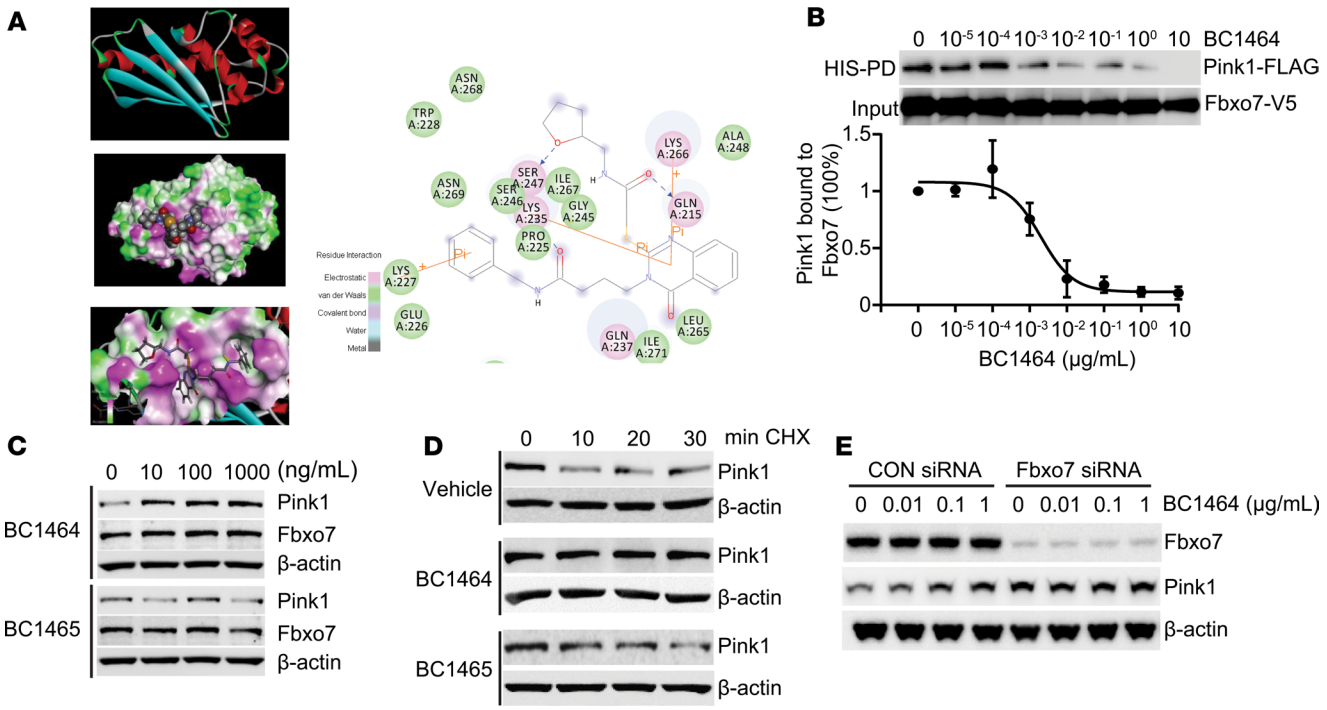

Figure 5. Fbxo7 FP domain small molecule inhibitor accumulates PINK1 protein. (**A**) Structural analysis of the Fbxo7 FP domain. Docking study of a candidate inhibitor BC1464 within the Fbxo7-FP domain suggests hydrophilic interactions of residues GLN215, LYS235, and LYS266 with BC1464. (**B**) His pull down Fbxo7 protein was exposed to BC1464 at indicated concentrations. TnT-synthesized PINK1 protein was then incubated with drug-bound Fbxo7 beads overnight. The eluate was subjected to immunoblotting. The relative amounts of PINK1 detected in the pull-downs were normalized to loading and quantified; data are shown as means ± SEM (n = 3). (**C**) BEAS-2B cells were incubated with BC1464 or the control compound BC1465 at the indicated concentrations for 16 hours before immunoblotting. (**D**) BEAS-2B cells were pretreated with BC1464 or BC1465 (1 μg/mL) for 16 hours, and the cells were then incubated with CHX (40 μg/mL). The cells were collected at indicated time points for immunoblot analysis. (**E**) BEAS-2B cells were nucleofected with control or Fbxo7 siRNA (50 pg) and incubated for 72 hours. BC1464 was then administrated at indicated concentration for an additional 18-hour incubation. The cell lysates were subjected to immunoblotting.

We found that BC1464 was able to not only reduce cell death (Figure 8I), but also protect against retraction and simplification of the dendritic arbor (Figure 9).

We obtained fibroblasts from control and 2 Parkinson's disease patients with mutations in leucine-rich repeat kinase (LRRK2) linked to an autosomal dominant form of Parkinson's disease (38, 39). We found that BC1464 conferred significant protection against a second Parkinsonian toxin 6-hydroxydopamine (6-OHDA) (40) in these primary human fibroblast cultures (Figure 10A). Moreover, neuroprotection was maintained even when BC1464 was applied 6 hours after either MPP+ or 6-OHDA (Figure 10, B and C, and Supplemental Figure 4). As a control for possible transcriptional effects of BC1464 in the primary fibroblasts, we performed quantitative reverse transcription PCR (RT-qPCR) and found no effects on either PINK1 or FBXO7 mRNA levels (Figure 10D). Finally, we found that BC1464 protects against parkinsonian cell death in neural progenitor cells differentiated from induced pluripotent stem cells (iPSC) from a familial Parkinson's disease patient with triplication of the *SNCA* gene (Figure 10, E and F). Taken together, these data indicate that BC1464 stabilizes PINK1 expression, increases markers of PINK1 activity within cells, and exerts cytoprotective activity in a variety of human and mouse cell types and injury models.

Discussion

Mitochondria have long been appreciated as essential effectors of cellular processes beyond energy production. Our discovery that the ubiquitin E3 ligase subunit FBXO7 targets prosurvival, antiinflammatory PINK1 for degradation led us to the development of a mitochondrial protective therapeutic small molecule compound. This FBXO7-targeted small molecule, which disrupts the interaction between PINK1 and FBXO7, protects cells and mice from inflammatory injury induced by endotoxin and bacterial infection. Moreover, BC1464 shows striking neuroprotective effects in cellular models of Parkinson's disease.

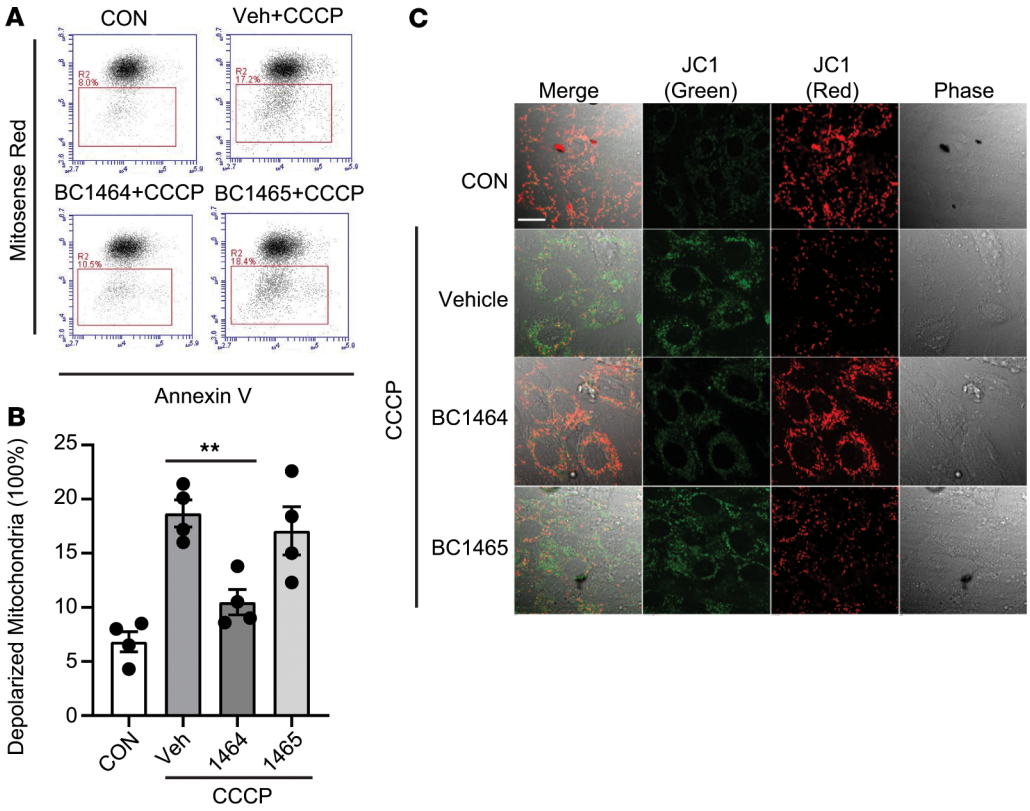

Figure 6. Fbxo7 FP domain small molecule inhibitor reduces mitochondrial depolarization. (**A**) H9C2 cells were treated with BC1464 or BC1465 (100 ng/mL) for 16 hours, with CCCP (20 μM) for an additional 2 hours, and then stained with MitoSense Red and annexin V before flow cytometry analysis. (**B**) Depolarized mitochondria percentage was quantified; data are shown as means ± SEM (n = 4). (**C**) H9C2 cells were treated with BC1464 or BC1465 (100 ng/mL) for 16 hours and then were treated with CCCP (20 μM) for an additional 2 hours. Cells were stained with JC1 (2 μM) for 20 minutes before confocal microscopy analysis. Scale bar: 10 μm. $^{**}P < 0.01$, as indicated by 1-way ANOVA with Tukey's test of multiple comparisons (**B**).

As both PINK1 and FBXO7 proteins have varied functions depending on species, tissue, or cellular contexts, there are several potential mechanisms underlying the ability to regulate mitochondrial function and modulate Parkinson's disease pathogenesis. One of the functions of PINK1 involves recruitment of Parkin to depolarized mitochondria to initiate the ubiquitin pathway of mitophagy (Reviewed in ref. 41). In fibroblasts and neuroblastoma cell lines, FBXO7 functions downstream of PINK1 to enhance Parkin recruitment (26). Theoretically, inhibiting mitophagy may comprise an undesired side effect of inhibiting FBXO7. However, the PINK1-parkin pathway is not necessary for receptor-mediated mitophagy (42), cardiolipin-mediated mitophagy (43), or mitophagy in brain tissues in vivo (44, 45). These data suggest that inhibiting FBXO7 may be well tolerated due to redundancy in mitophagy mechanisms.

Our data indicate that PINK1 is degraded through interaction with FBXO7. Thus, FBXO7 functions not only to facilitate mitophagy downstream of PINK1 (26), but also to downregulate PINK1 itself. This may serve as a feedback mechanism to terminate the acute mitophagy response. Given that sustained mitophagy that leads to mitochondrial depletion is harmful to neurons (46–48), activation of a feedback mechanism to limit the extent of mitochondrial clearance may be particularly important in the nervous system.

Other potential mechanisms by which elevating PINK1 may protect against neurodegeneration include its ability to suppress apoptosis (49), mitochondrial oxidative stress (12, 50, 51), and mitochondrial calcium overload (52, 53). PINK1 also acts to enhance mitochondrial complex I activity (54) and mitochondrial transport into dendrites (15, 16). Recently, it has been shown that PINK1 plays a prodifferentiation role in neurons, interacting with valosin-containing protein to promote dendritic arborization through PKAc-mediated phosphorylation of p47 (13).

Through its role in mitochondrial quality control, PINK1 may prevent the release of danger signals from damaged mitochondria or act directly to regulate inflammatory cell function (55, 56). We cannot

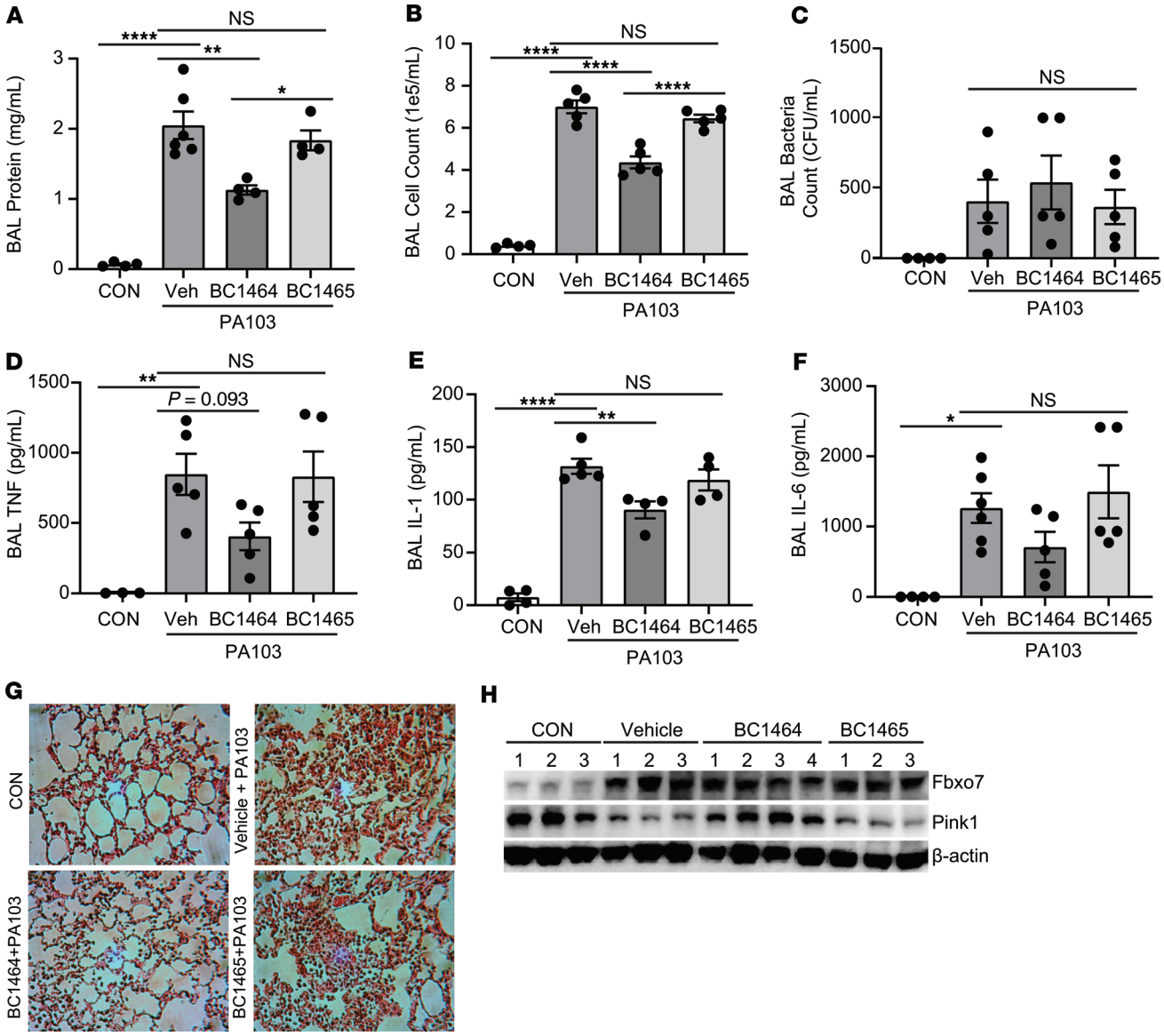

Figure 7. Fbxo7 small molecule inhibitor attenuates severity of experimental lung inflammation. C57BL/6N mice (5–6 mice/group) were administered i.t. with PA103 (1×10^4 PFU/mouse). BC1464 was given through an i.p. injection (5 mg/kg) at the same time. Compound BC1465 served as a negative control. 18 hours later, mice were euthanized, and lungs were lavaged with saline, harvested, and then homogenized. (**A–F**) Lavage protein, cell count, bacteria loads, and cytokine secretion were measured. (**G**) H&E staining was performed on lung samples; original magnification, 100×. Data are shown as means ± SEM of 4–6 mice/group. (**H**) Mice lung tissue from each group was homogenized and subjected to immunoblotting analysis. *$P < 0.05$, **$P < 0.01$, ****$P < 0.0001$, as indicated by 1-way ANOVA with Tukey's test of multiple comparisons (**A–F**).

exclude the possibility that, aside from PINK1, other yet-unknown substrates targeted by FBXO7 may also regulate mitochondria, neuritic branching, and inflammation. FBXO7 elevates NF-κB activity through inhibition of cIAP1 and TRAF2. NF-κB inhibitors have been proposed as treatments for both Parkinson's disease and for inflammatory lung disease. Notably, PINK1 plays an important role in limiting inflammation in multiple tissues in vivo. PINK1 deficiency results in increased T cell responses to gram-negative gut bacteria, triggering autoimmune mechanisms in both the periphery and the brain to cause motor symptoms (57).

In conclusion, with its neuroprotective, mitoprotective, prosurvival, and antiinflammatory effects, elevating PINK1 represents a promising therapeutic goal. Not only are destabilizing mutations implicated for Parkinson's disease (58), but WT PINK1 expression is also reduced in brains of patients with Alzheimer's disease (59), the muscle of patients with diabetes (60), and the lungs of patients with age-related idiopathic pulmonary fibrosis (30). The identification of an F-box protein–targeted small molecule antagonist capable

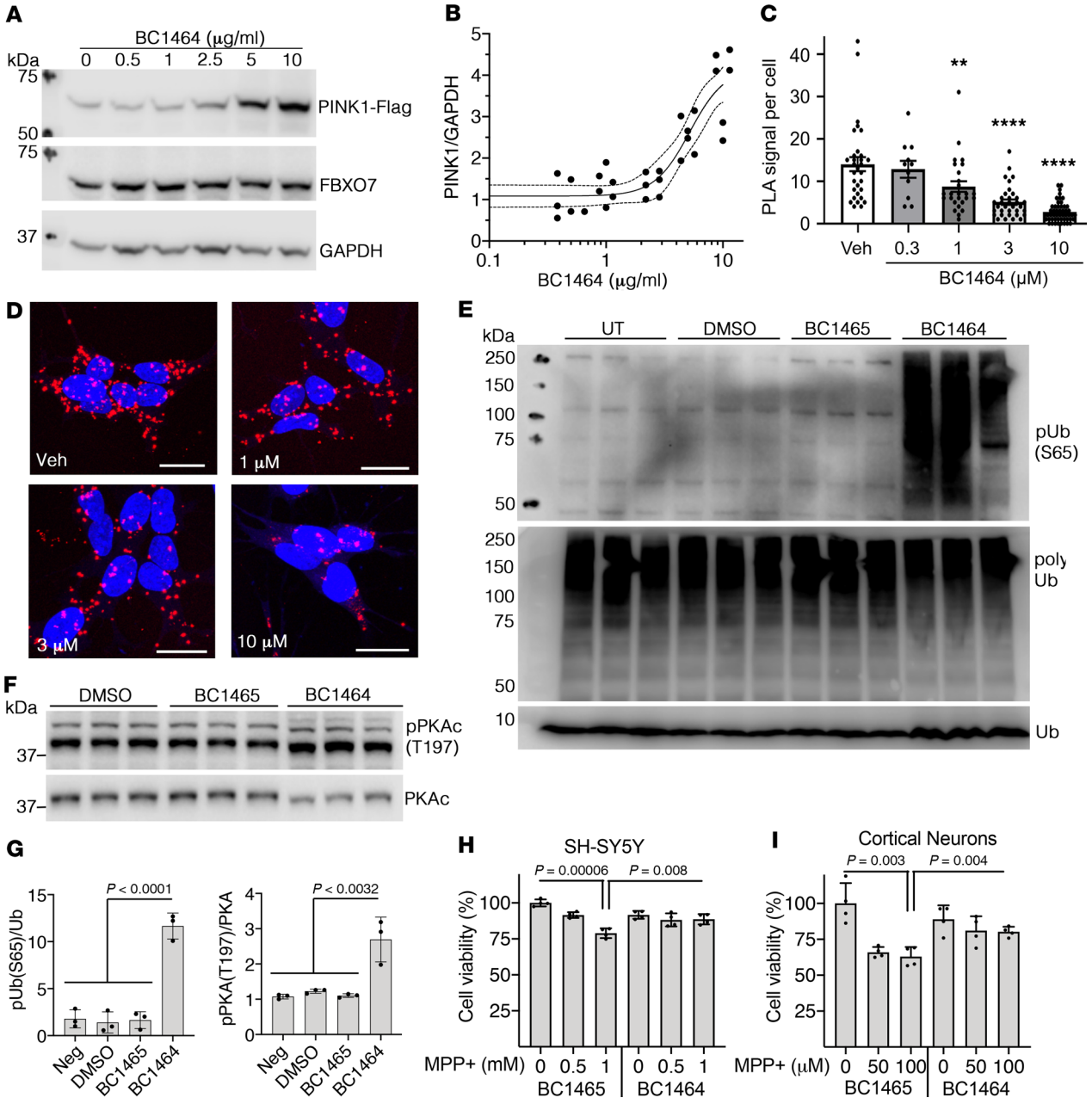

Figure 8. Fbxo7 small molecule inhibitor elevates PINK1 and protects against MPP+ toxicity in human cells and primary neurons. (**A**) Human SH-SY5Y cells stably expressing PINK1-FLAG were treated with the indicated amounts of BC1464 for 3 hours, followed by incubation for 1 hour in the presence of CHX (10 μg/mL) before immunoblotting analysis. (**B**) Densitometry analysis revealed an IC_{50} of ~5.2 μg/mL by nonlinear regression (n = 6; interpolated mean with 95% CI bands; Prism v 8.2.1, 2019, sigmoidal 4PL; 32 Degrees of Freedom, R^2 = 0.81; Hill coefficient = 2.9). (**C** and **D**) Duolink Proximity Ligation Assay of Fbxo7 and PINK1-FLAG in SH-SY5Y cells treated with BC1464 titration. EC_{50} ~1.4 μM by nonlinear regression (mean ± SEM; $^{**}P < 0.01$; $^{***}P < 0.001$; $^{****}P < 0.0001$ vs. vehicle by 1-way ANOVA with Dunnett's post hoc test). PLA is detected with red fluorescence, and nuclei counterstained using Hoescht 33342. Scale bar: 20 μm. (**E–G**) SH-SY5Y cells were treated with vehicle or the indicated compound (5 μg/mL) for 16 hours and then lysed for Western blot for ubiquitin phosphorylated at S65 (**E**) and phosphorylated PKAc (**F**). (**G**) Densitometric analysis of the indicated phospho-epitopes. (mean ± SD, n = 3 wells, representative of 2 independent experiments; 1-way ANOVA with Bonferroni's post hoc test). (**H**) SH-SY5Y cells were treated with the indicated concentrations of MPP+ or vehicle control in the presence of 5 μg/mL BC1465 or BC1464 for 24 hours. Cell viability was measured using AlamarBlue fluorescence intensity. (**I**) Mouse E16 primary cortical neurons were treated with the indicated concentrations of MPP+ in the presence of either 5 μg/mL BC1465 or BC1464 for 24 hours, and cell numbers were measured as in **H**. Data in **H** and **I** are shown as mean ± SD; n = 4 independent experiments; 1-way ANOVA with Bonferroni-corrected 2-tailed t test.

of restoring PINK1 concentrations in cells fulfills a void in the preclinical arena with implications for neurodegenerative, proinflammatory, and mitochondrial disorders. These data set the stage for additional target validation and lead optimization work for the potential treatment of a range of neurodegenerative and other diseases characterized by dysregulation of mitochondrial function and/or inflammation.

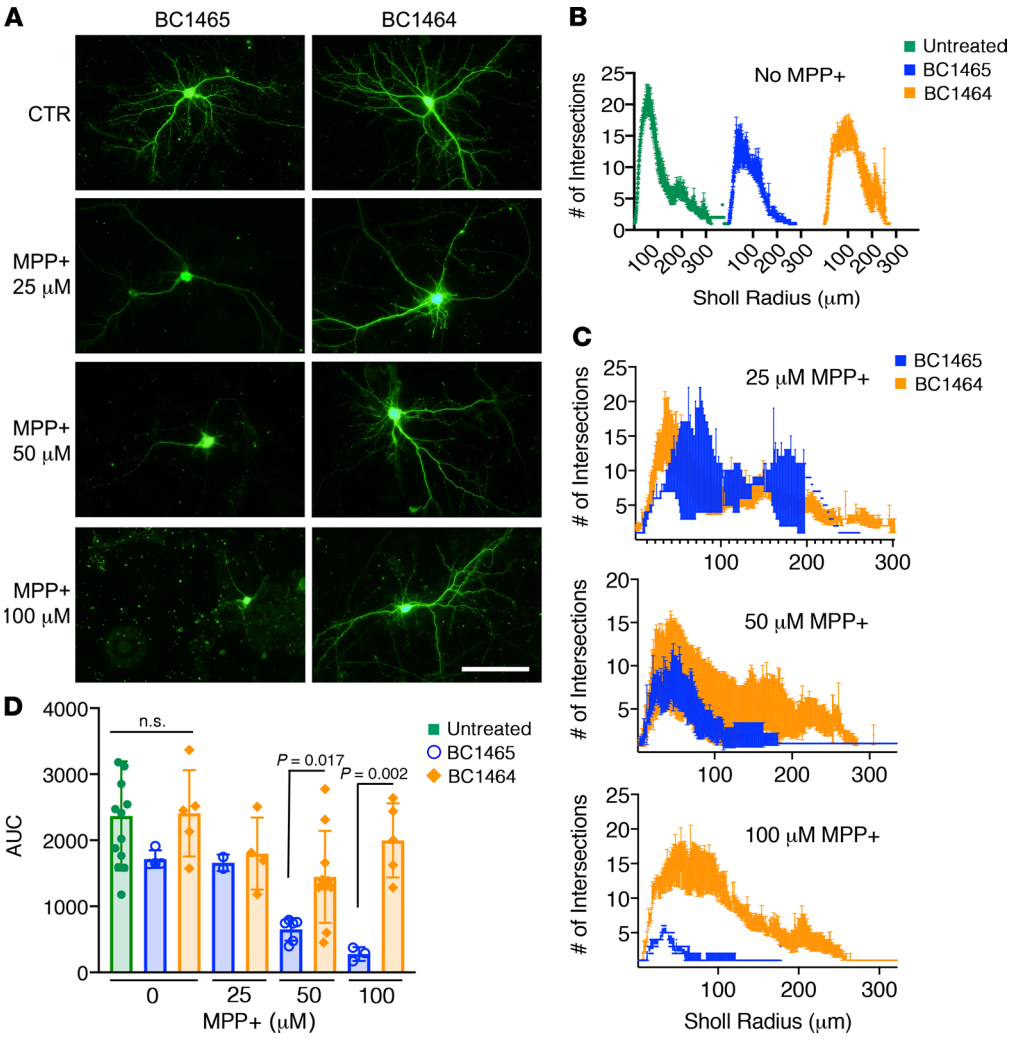

Figure 9. Fbxo7 small molecule inhibitor protects neuronal arborizations against MPP+ injury. (**A**) Mouse E16 primary cortical neurons were transfected with GFP on day 7 and then treated on day 14 with 5 μg/mL BC1465 or BC1464 before being challenged with the indicated concentrations of MPP+ for 24 hours. Scale bar: 100 μm. (**B** and **C**) Neurons were assessed for morphological injury using Sholl analysis with a radius step size of 1 μm (mean ± SEM of individual neuron traces). (**D**) The AUC was calculated for each neuron analyzed (mean ± SD, *n* = 3–10/group, 1-way ANOVA with post hoc Bonferroni-corrected 2-tailed *t* test).

Methods

Cell culture and transfection. Murine lung epithelial (MLE12) cells (ATCC) and human bronchial epithelial (BEAS-2B) cells (ATCC) were cultured with HITES medium (DMEM/F12 supplemented with insulin, transferrin, hydrocortisone, β-estradiol, and glutamine) containing 10% FBS and antibiotics as described previously (61). For $t_{½}$ studies, cells were treated with CHX (40 μg/mL) in blank medium and collected at different time points. Cell lysates were prepared by brief sonication in RIPA buffer including 150 mM NaCl, 50 mM Tris, 1.0 mM EDTA, 2 mM dithiothreitol, and 0.025% sodium azide, supplemented with Pierce protease inhibitor tablets (Thermo Fisher Scientific) at 4°C. All plasmids were delivered into cells using nucleofection following manufacturer's protocols (Lonza). All plasmid constructs were generated using PCR-based strategies with appropriate primers; point mutants were generated using site-directed mutagenesis kit (62). Rat myoblast H9C2 cells (ATCC) were cultured in DMEM medium supplemented with 10% FBS and antibiotics. SH-SY5Y cells (ATCC) were maintained in antibiotic-free DMEM medium supplemented with 10% FBS, 2 mM L-glutamine, and 10 mM HEPES in a humidified incubator at 37°C and 5% CO_2. Primary fibroblasts and an iPSC line from a PD patient with SNCA gene triplication were purchased from the NINDS Human Cell and Data Repository at Rutgers University (RUCDR Infinite Biologics). Timed pregnant female C57BL/6N mice were purchased from Charles River Laboratories. Primary E16

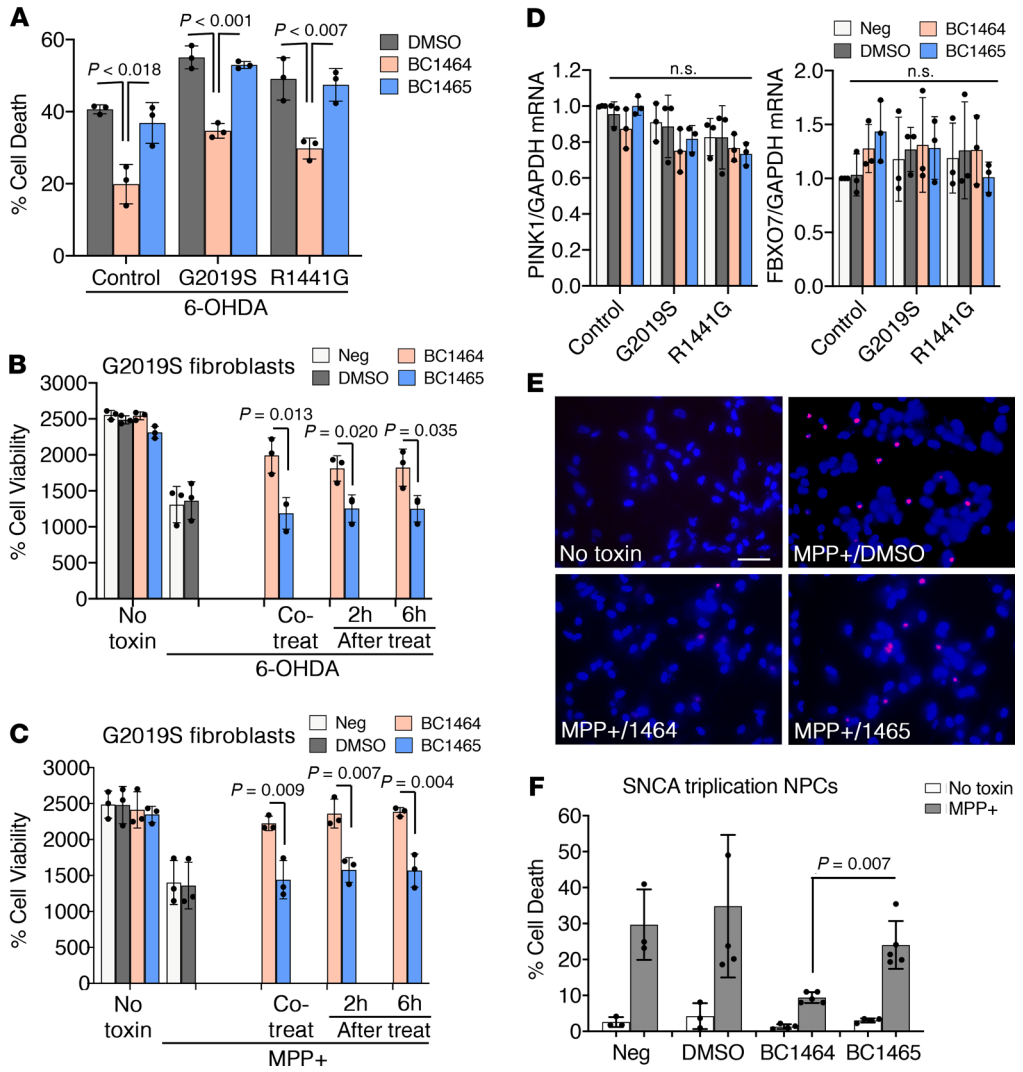

Figure 10. Fbxo7 small molecule inhibitor protects human patient cells against PD toxins. (**A**) Primary fibroblasts from a control subject and 2 Parkinson's disease patients, one with the G2019S mutation and the other with the R1441G mutation of LRRK2, were treated with 6-OHDA for 16 hours in the presence of DMSO, BC1464, or BC1465 and cell death percentage assessed. (**B** and **C**) Fibroblasts from a LRRK2-G2019S patient were treated with 6-OHDA or MPP+, with BC1464 or BC1465 added simultaneously or 2–6 hours later. Similar results were obtained for the other fibroblast lines (Supplemental Figure 4). Mean ± SD, n = 3 independent experiments, ANOVA with post hoc 2-tailed t test for **A–C**. (**D**) The fibroblasts from each subject were treated with DMSO vehicle, BC1464, and BC1465 and analyzed for PINK1 and FBXO7 mRNA by RT-qPCR (mean ± SD, n = 3 independent experiments, 1-way ANOVA, $P > 0.548$). (**E** and **F**) Late NPCs from SNCA triplication iPSC line were treated with Neurobasal media (Neg), DMSO, BC1464, or BC1465 as indicated and analyzed for cell death using propidium iodide (mean ± SD, n = 3–5 independent experiments, ANOVA with post hoc t test). Scale bar: 100 μm.

cortical neurons were isolated as previously described (13), plated at 150,000–200,000 cells/cm^2 in LabTek II coverglass chamber slides or tissue culture plates coated with poly-L-lysine (0.1 mg/mL), and maintained in antibiotic-free neurobasal (NB) medium supplemented with 2% B27 and 2 mM glutamax (Thermo Fisher Scientific). SH-SY5Y cells and cortical neurons in 96-well plates were treated with the indicated concentrations of MPP+ and 5 μg/mL of either BC1464 or BC1465. Fibroblasts were treated with MPP+ (400 μM) or 6-OHDA (300 μM), and BC1464 or BC1465 were added 0–6 hours after the toxin. After 24 hours, cell viability was analyzed using the alamarBlue Assay according to the manufacturer's instructions (Bio-Rad Laboratories). Late neural progenitor cells were derived as previously described (63). Briefly, iPSCs were differentiated into neural stem cells (NSCs)/ectodermal neural progenitor cells (eNPCs) by manual fragmentation and culture in ultra-low attachment plates; they were then transferred to Matrigel-coated Ibidi plates (Ibidi, 80426) and seeded at about 33,000 cells/mL. eNPCs were cultured for an additional 3 weeks in NB

media (Thermo Fisher Scientific, 21103049) supplemented with B27 and BDNF (Invitrogen, RP8642) to obtain late NPCs, with NB media change every other day, and treated with BC1464, BC1465, DMSO vehicle (MilliporeSigma, D2660), or NB media for 1 week. Cells were stained with propidium iodide for analysis of nuclear morphology, and images were acquired with a 40× oil objective (1.30 NA) on an Olympus IX71 microscope using Olympus CellSens V1.17 with a DP80 camera. Primary cortical neurons were transfected with IRES-GFP (gift from Dennis Selkoe, Harvard University, Cambridge, Massachusetts, USA) at 7 days in vitro (DIV7), allowed to mature to DIV14, and then treated with 5 μg/mL of BC1464 or BC1465 four hours before addition of MPP+. After 24 hours, cultures were analyzed for propidium iodide exclusion or processed for morphological analysis as described below. If not otherwise specified, all chemicals were obtained from MilliporeSigma, and culture media was from Lonza. BC1464 and BC1465 are from ChemDIV Inc.

Molecular docking studies and compound screening. The docking experiments were performed using software from Discovery Studio 3.5. A library containing 3 million compounds was first used to screen potential ligands for Fbxo7 FP domain. FP domain structural analysis revealed a major drug-binding cavity. The binding cavity was adopted into the LibDock algorithm to screen for the optimum inhibitor. Based on the docking and best-fit analysis of suitable ligands, BC-1464 was selected and tested as the hit compound.

Reagents. The pcDNA3.1D/V5-His-TOPO cloning kit, V5 antibody (R960-25), and *E. coli* Top10 One-Shot-competent cells were from Invitrogen. Leupeptin, MPP+, anti-FLAG (M2) (F1804), Duolink Proximity Ligation Assay Kit (DUO92102), and CCCP were from MilliporeSigma. PINK1 rabbit antibody (BC100-494) was from Novus Biologicals. Anti-Fbxo7 (10696-1-AP) was from Proteintech. Phospho–PKA-C(T197) (catalog 4781) and phospho-Ubiquitin (S65) (catalog 62802) antibodies were from Cell Signaling Technology. β-Actin mouse monoclonal antibody (sc-81178) and PKAα/β/γ cat (catalog 98951) were from Santa Cruz Biotechnology Inc. Ubiquitin antibody (Z0458) was from Dako. GAPDH antibody (ab37168) was from Abcam. MG-132 was from UBPBio. Protease inhibitor tablets and Supersignal West Femto chemiluminescent substrate were from Thermo Fisher Scientific. The Fbxo7 cDNA, PINK1 cDNA, scrambled shRNA, and human and mouse Fbxo7 shRNAs were from OpenBiosystems. Nucleofector transfection kits were from Amaxa. QuikChange site-directed mutagenesis kits were from Agilent. Immobilized protein A/G beads were from Pierce. Purified Cul1, Rbx1, and Skp1 were from Abnova. Purified ubiquitin, E1, E2, and ubiquitin aldehyde were from Enzo Life Sciences. CHX was from Calbiochem. Fbxo7 rabbit antibody (ARP43128_P050) was from Aviva Systems Biology. TNT quick-coupled transcription/translation systems were from Promega. The RNA purification kit was from QIAGEN. RNA was purified using the RNeasy mini kit (74104, QIAGEN). The SuperScript IV VILO RT Master Mix (Invitrogen, 11756050) was used for reverse transcription. Quantitative PCR (qPCR) was performed using TaqMan qPCR reagents: qPCR master mix solution (Applied Biosystems, 4369016) and TaqMan probes for PINK1 (Applied Biosystems, Hs00260868_ml), FBX07 (Applied Biosystems, Hs00201825_ml), and GAPDH (Applied Biosystems, Hs02786624_g1).

Mass spectrometry. GFP IP products from HEK293 cells expressing either EGFPc-1 or WT-PINK1-GFP, isolated using the μMACS Epitope Tag Protein Isolation Kit (Miltenyi Biotec), were electrophoresed into a stacking gel. Resulting gel bands were excised, destained in 100 mM ammonium bicarbonate, reduced in 5 mM DTT, and alkylated in 15 mM iodoacetamide as previously described (64). Gel spots were washed in 50% acetonitrile/100 mM AMBIC and incubated overnight in 0.05 μg/μL trypsin in 100 mM AMBIC at a 1:100 enzyme to protein ratio. Digested peptides were extracted in 60% acetonitrile/0.1% trifluoroacetic acid before being lyophilized and resuspended in 5% formic acid. An EASY-nLC II liquid chromatography system was used to separate peptides. High-resolution peptide precursor measurements were made in the Orbitrap (R = 60,000 at 400 *m/z*), and low-resolution peptide fragment ion spectra were collected by collision-induced dissociation in the dual-linear ion trap of an Orbitrap Elite Mass Spectrometer. Data were searched using SEQUEST against a UniProt-derived human protein database (downloaded 01/17/2011; https://www.uniprot.org/) that contained 67,173 TrEMBL and Swiss-Prot human protein entries further amended with an entry for GFP. Fold-change ($\log_2$) ratios were calculated following addition of 0.5 to summed peptide spectral matches (PSMs) for corresponding protein identifications to enable comparative analyses of "presence-absence" scenarios.

Mutants. All Fbxo7 mutant constructs were generated by site-directed mutagenesis using the site-directed mutagenesis kit (Agilent).

Flow cytometry. Transfected cells were incubated with MitoTracker Red (50 nM) for 15 minutes following the protocols of the manufacturer (Invitrogen). Cells were washed with medium 4 times before harvesting with trypsin digestion. Cell suspensions were then analyzed with an AccuriC6 system with De Novo software. MitoTracker staining was measured by flow cytometry FL1 (FITC;

excitation wavelength, 488 nm; emission wavelength, 530 nm) and FL3 (MitoTracker Red; excitation wavelength, 488 nm; emission wavelength, 610 nm) with unstained cells serving as negative controls. The enclosed areas represent the percentage of defective mitochondria.

Immunoblotting and IP. Whole cell extracts (normalized to total protein concentration) were subjected to SDS-PAGE, electrotransferred to membranes, and immunoblotted. For IP, 1 mg of cell lysates (in PBS with 0.5% Triton X-100 plus protease inhibitors) were incubated with 2 μg of V5 mouse antibodies for 3–4 hours at 4°C, followed by addition of 30 μL of protein A/G-agarose for an additional 1 hour at 4°C. The precipitated complex was washed 3 times with 0.5% Triton X-100 in PBS and analyzed by immunoblotting with an enhanced ECL system.

Duolink PLA. PLA was conducted using Duolink technology, according to manufacturer's protocol (MilliporeSigma). Briefly, SH-SY5Y cells stably expressing PINK1-FLAG were seeded to 96-well glass bottom plate (Cellvis) and treated with a titration of BC1464 for 18 hours before fixation with 4% paraformaldehyde for 1 hour. Cells were permeabilized with 0.5% Triton-X-100 for 0.5 hours and blocked with Duolink Blocking solution at 37°C for 2 hours. Anti-Fbxo7 (Proteintech, 10696-1-AP) and anti-FLAG (M2) (MilliporeSigma, F1804) antibodies were incubated with cells overnight. PLA probe incubation (secondary antibody), ligation, and amplification were conducted according to manufacturer's protocol. Cells were counterstained with Hoescht 33342 (Invitrogen). Fluorescence was measured and processed with Cytation5 high content imager (BioTek), and the PLA signal per cell was calculated using CellProfiler (65). Representative confocal images were taken using a Leica SP8 confocal microscope.

In vitro ubiquitylation assays. The ubiquitylation of WT or lysine mutant PINK1-V5 was performed in a volume of 20 μL containing 50 mM Tris (pH 7.6), 5 mM $MgCl_2$, 0.6 mM DTT, 400 μM MG132, 2 mM ATP, 50 nM E1, 0.5 μM UbcH5, 0.5 μM UbcH7, 2 μM ubiquitin, 1 μM ubiquitin aldehyde, 20 nM Cul1, 20 nM Rbx1, 20 nM Skp1, in vitro–synthesized PINK1-HA (WT or mutant), and Fbxo7 within the TNT-coupled reticulocyte lysate system. Reaction products were examined for HA immunoblotting.

PA103 infection. PA103 inoculums were freshly prepared before experiments using frozen stocks of *P. aeruginosa* (ATCC strain 29213, frozen at mid-log phase; OD625 = 0.8). *P. aeruginosa* was maintained in tryptic soy broth minimal agar. Cultures were plated and grown overnight from frozen stock. Overnight plate cultures were then inoculated in tryptic soy broth and grown by rotary shaking at 37°C to log phase. Cells were then infected with *P. aeruginosa* at multiplicity of infection (MOI) of 10, 50, or 100 for 1, 2, or 16 hours.

Co-IP. A total of 500 μg of total protein from cell lysates was precleared with 20 μL of protein A/G beads for 1 hour at 4°C. A total of 2 μg of primary antibody was added to TnT synthesized PINK1 for 18-hour incubation at 4°C. A total of 20 μL of protein A/G beads was added for an additional 6 hours of incubation. Beads were slowly centrifuged at 500 *g* for 2 minutes and washed 5 times using 50 mM HEPES, 150 mM NaCl, 0.5 mM EGTA, 50 mM NaF, 10 mM Na_3VO_4, 1 mM phenylmethylsulfonyl fluoride, 20 μM leupeptin, and 1% (v/v) Triton X-100 (radio-IP assay) buffer, as described (66). The beads were heated at 100°C for 5 minutes with 80 μL of protein sample buffer before SDS-PAGE and immunoblotting.

Microscopy and immunostaining. Microscopy work was performed using a Nikon A1 confocal microscope with a 60× oil objective. The microscope was equipped with Ti Perfect Focus system and Tokai Hit live cell chamber providing a humidified atmosphere at 37°C with 5% CO_2. Nucleofected cells (2×10^5) were plated at 70% confluence on 35 mm MatTek glass-bottom culture dishes, treated with or without CCCP, and labeled with either MitoTracker Red (50 nM) or JC1 (2 μM) for an additional 20 minutes. Image analysis was performed by Nikon NIS-element and ImageJ (NIH) software. Pseudocolor green was used for optimal resolution of mitochondria MitoTracker image display. Primary neurons were fixed in 2% paraformaldehyde at room temperature for 20 minutes, washed 3× in PBS, permeabilized with 0.5% triton-X 100 for 10 minutes, and washed 4×. After 1 hour, in SuperBlock and washing 3× in PBS with 0.1% Tween-20, neurons were incubated with rabbit anti-GFP (Invitrogen, A6455) at 1:1000 for 1 hour, washed 4×, and incubated with Alexa 488–conjugated secondary antibody (Invitrogen, A-11008) at 1:500 for 1 hour. Morphological injury was assessed by Sholl and AUC analysis.

Animal studies. Male C57LB/6 mice (purchased from the Jackson Laboratory) were acclimated at the University of Pittsburgh Animal Care Facility and maintained according to all federal and institutional animal care guidelines and under a University of Pittsburgh IACUC-approved protocol. Mice were deeply anesthetized with ketamine (80–100 mg/kg of body weight, i.p.) and xylazine (10 mg/kg, i.p.); then, the larynx was well visualized under a fiber optic light source before endotracheal intubation with a 24-gauge plastic catheter. Replication-deficient lentivirus (Lenti) alone or Lenti-*Fbxo7*, Lenti-shRNA control, or Lenti-shRNA

Fbxo7 (1×10^8 plaque-forming units in 50 μL of PBS) was instilled i.t. on day 1, after which animals were allowed to recover for 7 days before bacterial infection (67). For the drug treatment studies, compound solutions were prepared in corn oil with brief sonication (final concentration, 1.5mg/mL), with 100 μL injected i.p. following bacterial infection. Mice were euthanized 18 hours after bacterial infection. The BAL fluids were analyzed by immunoblotting, cell count, and cytokine ELISA with H&E staining of lung tissue.

Human lung explants. Donor human lungs not accepted for transplant were obtained through the University of Pittsburgh Committee for Oversight of Research and Clinical Training Involving Decedents (CORID). Donor medical records were deidentified, and IRB approval is not required to access these tissues. Organs were considered appropriate for study if there was no evidence of parenchymal lung disease, gas exchange was within normal limits before harvest, and organs could be processed with less than 6 hours cold ischemic time. Localized lesions (e.g., solitary nodules) were avoided during tissue selection. Single lung segments were dissected and warmed in a weighted plastic bag in a 37°C water bath for 30 minutes. A 2% low melting point agarose in PBS (Invitrogen Ultrapure) is also maintained at 37°C. The lung segments were filled with agarose by instillation into airways via syringe with 18-gauge cannula and inspected for appropriate expansion, followed by airway clamping. Tissue was placed in a bag and submerged in ice for 30 minutes or until the agarose had set. Tissue was cut to block size (2 cm × 1 cm × 1 cm) and sliced in ice cold saline with a vibratome (Leica VT 1200) at slice thickness of 300 μm. Uniform slices were sectioned into 1 cm × 1 cm sections and cultured in RPMI containing penicillin-streptomycin and Amphotericin B (Thermo Fisher Scientific) without serum in 12-well dishes at 37°C in a tissue incubator with 5% CO_2. Medium was changed after 2 hours, and experiments were performed in 1 mL media after overnight incubation. Slices were treated with the indicated concentrations of test compounds and simultaneously exposed to 50 ng/mL LPS for 4 hours before homogenization and resuspension in lysis buffer.

Statistics. Statistical analysis was performed with 1-way ANOVA followed by post hoc Dunnett's or Bonferroni-corrected 2-tailed *t* tests. F-test was used to compare variances. $P < 0.05$ were considered significant.

Study approval. Procedures for the derivation of primary neuron cultures were approved by the University of Pittsburgh IACUC. Mice were maintained according to all federal and institutional animal care guidelines under a protocol approved by the University of Pittsburgh IACUC. Donor human lungs not accepted for transplant were obtained through the University of Pittsburgh CORID. Donor medical records were deidentified, and IRB approval is not required to access postmortem tissues.

Author contributions

YL conducted experiments, analyzed data and wrote the manuscript. TBL, MV, KZQW, PAO, ACM, SRD, ES, NWB, YJ, NMW, and MR conducted experiments and analyzed data. CW directed the mass spectrometry work. CTC, BBC, and RKM directed the overall study, designed experiments, and wrote the manuscript.

Acknowledgments

We thank Shristi Rajbhandari, Olivia Iannone, Jason Callio, and Jacob Jerome for technical assistance. This work was supported, in part, by American Heart Association Scientist Development Grant 16SDG27650008 (YL). This work was supported, in part, by NIH grants HL096376, HL097376, HL098174, HL081784, and P01 HL114453 (RKM); AG026389, NS101628 (cofunded by NINDS/NIA), and NS065789 (CTC); HL139860 and HL133184 (BBC); and HL142777 (YL). The content is solely the responsibility of the authors and does not necessarily represent the official views of the NIH. This work was also supported, in part, by the United States Department of Veterans Affairs, Veterans Health Administration, Office of Research and Development, Biomedical Laboratory Research and Development, a Merit Review Award from the United States Department of Veterans Affairs (RKM), and the Helen Mendel Fund (CTC).

Address correspondence to: Charleen T. Chu, S701 Scaife Hall, 3550 Terrace Street, Department of Pathology, University of Pittsburgh School of Medicine, Pittsburgh, Pennsylvania 15261, USA. Phone: 412.383.5379; Email: ctc4@pitt.edu. Or to: Bill B. Chen, Pulmonary, Allergy and Critical Care Medicine, BST-1 Room W1254, The University of Pittsburgh, Pittsburgh, Pennsylvania 15213, USA. Phone: 412.624.4404; Email: chenb@upmc.edu. Or to: Rama K. Mallampalli, Department of Internal Medicine, The Ohio State University, Wexner Medical Center, 395 W. 12th Avenue, Room 392, Columbus, Ohio 43210, USA. Phone: 614.293.8724; Email: rama.mallampalli2@osumc.edu.

ES's present address is: LGC Genomics-Douglas Scientific, Alexandria, Minnesota, USA.

NWB's present address is: Gynecologic Cancer Center of Excellence, Women's Health Integrated Research Center, Annandale, Virginia, USA.

CW's present address is: Stratus Bioscience, Seattle, Washington, USA.

RKM's present address is: Department of Internal Medicine, The Ohio State University, Columbus, Ohio, USA.

1. Lazarou M, et al. The ubiquitin kinase PINK1 recruits autophagy receptors to induce mitophagy. *Nature*. 2015;524(7565):309–314.
2. Steer EK, Dail MK, Chu CT. Beyond mitophagy: cytosolic PINK1 as a messenger of mitochondrial health. *Antioxid Redox Signal*. 2015;22(12):1047–1059.
3. Amo T, et al. Mitochondrial membrane potential decrease caused by loss of PINK1 is not due to proton leak, but to respiratory chain defects. *Neurobiol Dis*. 2011;41(1):111–118.
4. Morais VA, et al. Parkinson's disease mutations in PINK1 result in decreased Complex I activity and deficient synaptic function. *EMBO Mol Med*. 2009;1(2):99–111.
5. Valente EM, et al. Hereditary early-onset Parkinson's disease caused by mutations in PINK1. *Science*. 2004;304(5674):1158–1160.
6. Mills RD, Sim CH, Mok SS, Mulhern TD, Culvenor JG, Cheng HC. Biochemical aspects of the neuroprotective mechanism of PTEN-induced kinase-1 (PINK1). *J Neurochem*. 2008;105(1):18–33.
7. Vincow ES, et al. The PINK1-Parkin pathway promotes both mitophagy and selective respiratory chain turnover in vivo. *Proc Natl Acad Sci USA*. 2013;110(16):6400–6405.
8. Büeler H. Impaired mitochondrial dynamics and function in the pathogenesis of Parkinson's disease. *Exp Neurol*. 2009;218(2):235–246.
9. Sha D, Chin LS, Li L. Phosphorylation of parkin by Parkinson disease-linked kinase PINK1 activates parkin E3 ligase function and NF-kappaB signaling. *Hum Mol Genet*. 2010;19(2):352–363.
10. Murata H, et al. A new cytosolic pathway from a Parkinson disease-associated kinase, BRPK/PINK1: activation of AKT via mTORC2. *J Biol Chem*. 2011;286(9):7182–7189.
11. Plun-Favreau H, et al. The mitochondrial protease HtrA2 is regulated by Parkinson's disease-associated kinase PINK1. *Nat Cell Biol*. 2007;9(11):1243–1252.
12. Pridgeon JW, Olzmann JA, Chin LS, Li L. PINK1 protects against oxidative stress by phosphorylating mitochondrial chaperone TRAP1. *PLoS Biol*. 2007;5(7):e172.
13. Wang KZQ, et al. PINK1 Interacts with VCP/p97 and Activates PKA to Promote NSFL1C/p47 Phosphorylation and Dendritic Arborization in Neurons. *eNeuro*. 2018;5(6):ENEURO.0466-18.2018.
14. Boonying W, et al. Pink1 regulates FKBP5 interaction with AKT/PHLPP and protects neurons from neurotoxin stress induced by MPP+. *J Neurochem*. 2019;150(3):312–329.
15. Dagda RK, et al. Beyond the mitochondrion: cytosolic PINK1 remodels dendrites through protein kinase A. *J Neurochem*. 2014;128(6):864–877.
16. Das Banerjee T, et al. PINK1 regulates mitochondrial trafficking in dendrites of cortical neurons through mitochondrial PKA. *J Neurochem*. 2017;142(4):545–559.
17. Sun L, Shen R, Agnihotri SK, Chen Y, Huang Z, Büeler H. Lack of PINK1 alters glia innate immune responses and enhances inflammation-induced, nitric oxide-mediated neuron death. *Sci Rep*. 2018;8(1):383.
18. Zhi L, et al. Loss of PINK1 causes age-dependent decrease of dopamine release and mitochondrial dysfunction. *Neurobiol Aging*. 2019;75.
19. Kim J, et al. PINK1 Deficiency Enhances Inflammatory Cytokine Release from Acutely Prepared Brain Slices. *Exp Neurobiol*. 2013;22(1):38–44.
20. Yamano K, Youle RJ. PINK1 is degraded through the N-end rule pathway. *Autophagy*. 2013;9(11):1758–1769.
21. Hershko A, Ciechanover A, Varshavsky A. Basic Medical Research Award. The ubiquitin system. *Nat Med*. 2000;6(10):1073–1081.
22. Hershko A, Ciechanover A. The ubiquitin system. *Annu Rev Biochem*. 1998;67:425–479.
23. Skowyra D, Craig KL, Tyers M, Elledge SJ, Harper JW. F-box proteins are receptors that recruit phosphorylated substrates to the SCF ubiquitin-ligase complex. *Cell*. 1997;91(2):209–219.
24. Tyers M, Willems AR. One ring to rule a superfamily of E3 ubiquitin ligases. *Science*. 1999;284(5414):601–604.
25. Nelson DE, Randle SJ, Laman H. Beyond ubiquitination: the atypical functions of Fbxo7 and other F-box proteins. *Open Biol*. 2013;3(10):130131.
26. Burchell VS, et al. The Parkinson's disease-linked proteins Fbxo7 and Parkin interact to mediate mitophagy. *Nat Neurosci*. 2013;16(9):1257–1265.
27. Zhao T, et al. Loss of nuclear activity of the FBXO7 protein in patients with parkinsonian-pyramidal syndrome (PARK15). *PLoS One*. 2011;6(2):e16983.
28. Yalcin-Cakmakli G, et al. A new Turkish family with homozygous FBXO7 truncating mutation and juvenile atypical parkinsonism. *Parkinsonism Relat Disord*. 2014;20(11):1248–1252.
29. Dagda RK, et al. Mitochondrially localized PKA reverses mitochondrial pathology and dysfunction in a cellular model of Parkinson's disease. *Cell Death Differ*. 2011;18(12):1914–1923.
30. Bueno M, et al. PINK1 deficiency impairs mitochondrial homeostasis and promotes lung fibrosis. *J Clin Invest*. 2015;125(2):521–538.
31. Shang J, Wang G, Yang Y, Huang X, Du Z. Structure of the FP domain of Fbxo7 reveals a novel mode of protein-protein interaction. *Acta Crystallogr D Biol Crystallogr*. 2014;70(Pt 1):155–164.

32. Kazlauskaite A, et al. Parkin is activated by PINK1-dependent phosphorylation of ubiquitin at Ser65. *Biochem J*. 2014;460(1):127–139.
33. Chu CT, Zhu JH, Cao G, Signore A, Wang S, Chen J. Apoptosis inducing factor mediates caspase-independent 1-methyl-4-phenylpyridinium toxicity in dopaminergic cells. *J Neurochem*. 2005;94(6):1685–1695.
34. Zhu JH, Gusdon AM, Cimen H, Van Houten B, Koc E, Chu CT. Impaired mitochondrial biogenesis contributes to depletion of functional mitochondria in chronic MPP+ toxicity: dual roles for ERK1/2. *Cell Death Dis*. 2012;3:e312.
35. Snyder SH, D'Amato RJ. MPTP: a neurotoxin relevant to the pathophysiology of Parkinson's disease. The 1985 George C. Cotzias lecture. *Neurology*. 1986;36(2):250–258.
36. Haque ME, et al. Cytoplasmic Pink1 activity protects neurons from dopaminergic neurotoxin MPTP. *Proc Natl Acad Sci USA*. 2008;105(5):1716–1721.
37. von Coelln R, Kügler S, Bähr M, Weller M, Dichgans J, Schulz JB. Rescue from death but not from functional impairment: caspase inhibition protects dopaminergic cells against 6-hydroxydopamine-induced apoptosis but not against the loss of their terminals. *J Neurochem*. 2001;77(1):263–273.
38. Anand VS, Braithwaite SP. LRRK2 in Parkinson's disease: biochemical functions. *FEBS J*. 2009;276(22):6428–6435.
39. Cherra SJ, Steer E, Gusdon AM, Kiselyov K, Chu CT. Mutant LRRK2 elicits calcium imbalance and depletion of dendritic mitochondria in neurons. *Am J Pathol*. 2013;182(2):474–484.
40. Chalovich EM, Zhu JH, Caltagarone J, Bowser R, Chu CT. Functional repression of cAMP response element in 6-hydroxydopamine-treated neuronal cells. *J Biol Chem*. 2006;281(26):17870–17881.
41. Chu CT. Mechanisms of selective autophagy and mitophagy: Implications for neurodegenerative diseases. *Neurobiol Dis*. 2019;122:23–34.
42. Koentjoro B, Park JS, Sue CM. Nix restores mitophagy and mitochondrial function to protect against PINK1/Parkin-related Parkinson's disease. *Sci Rep*. 2017;7:44373.
43. Chu CT, et al. Cardiolipin externalization to the outer mitochondrial membrane acts as an elimination signal for mitophagy in neuronal cells. *Nat Cell Biol*. 2013;15(10):1197–1205.
44. McWilliams TG, et al. Basal Mitophagy Occurs Independently of PINK1 in Mouse Tissues of High Metabolic Demand. *Cell Metab*. 2018;27(2):439–449.e5.
45. Lee JJ, et al. Basal mitophagy is widespread in *Drosophila* but minimally affected by loss of Pink1 or parkin. *J Cell Biol*. 2018;217(5):1613–1622.
46. Verma M, Wills Z, Chu CT. Excitatory Dendritic Mitochondrial Calcium Toxicity: Implications for Parkinson's and Other Neurodegenerative Diseases. *Front Neurosci*. 2018;12:523.
47. Cherra SJ, Steer E, Gusdon AM, Kiselyov K, Chu CT. Mutant LRRK2 elicits calcium imbalance and depletion of dendritic mitochondria in neurons. *Am J Pathol*. 2013;182(2):474–484.
48. Shi RY, Zhu SH, Li V, Gibson SB, Xu XS, Kong JM. BNIP3 interacting with LC3 triggers excessive mitophagy in delayed neuronal death in stroke. *CNS Neurosci Ther*. 2014;20(12):1045–1055.
49. Arena G, et al. PINK1 protects against cell death induced by mitochondrial depolarization, by phosphorylating Bcl-xL and impairing its pro-apoptotic cleavage. *Cell Death Differ*. 2013;20(7):920–930.
50. Dagda RK, Cherra SJ, Kulich SM, Tandon A, Park D, Chu CT. Loss of PINK1 function promotes mitophagy through effects on oxidative stress and mitochondrial fission. *J Biol Chem*. 2009;284(20):13843–13855.
51. Martin SA, Hewish M, Sims D, Lord CJ, Ashworth A. Parallel high-throughput RNA interference screens identify PINK1 as a potential therapeutic target for the treatment of DNA mismatch repair-deficient cancers. *Cancer Res*. 2011;71(5):1836–1848.
52. Kostic M, et al. PKA Phosphorylation of NCLX Reverses Mitochondrial Calcium Overload and Depolarization, Promoting Survival of PINK1-Deficient Dopaminergic Neurons. *Cell Rep*. 2015;13(2):376–386.
53. Huang E, et al. PINK1-mediated phosphorylation of LETM1 regulates mitochondrial calcium transport and protects neurons against mitochondrial stress. *Nat Commun*. 2017;8(1):1399.
54. Morais VA, et al. PINK1 loss-of-function mutations affect mitochondrial complex I activity via NdufA10 ubiquinone uncoupling. *Science*. 2014;344(6180):203–207.
55. Sliter DA, et al. Parkin and PINK1 mitigate STING-induced inflammation. *Nature*. 2018;561(7722):258–262.
56. Matheoud D, et al. Parkinson's Disease-Related Proteins PINK1 and Parkin Repress Mitochondrial Antigen Presentation. *Cell*. 2016;166(2):314–327.
57. Matheoud D, et al. Intestinal infection triggers Parkinson's disease-like symptoms in Pink1$^{-/-}$ mice. *Nature*. 2019;571(7766):565–569.
58. Moriwaki Y, et al. L347P PINK1 mutant that fails to bind to Hsp90/Cdc37 chaperones is rapidly degraded in a proteasome-dependent manner. *Neurosci Res*. 2008;61(1):43–48.
59. Du F, et al. PINK1 signalling rescues amyloid pathology and mitochondrial dysfunction in Alzheimer's disease. *Brain*. 2017;140(12):3233–3251.
60. Scheele C, et al. Altered regulation of the PINK1 locus: a link between type 2 diabetes and neurodegeneration? *FASEB J*. 2007;21(13):3653–3665.
61. Liu Y, et al. The Proapoptotic F-box Protein Fbxl7 Regulates Mitochondrial Function by Mediating the Ubiquitylation and Proteasomal Degradation of Survivin. *J Biol Chem*. 2015;290(19):11843–11852.
62. Chen BB, Mallampalli RK. Masking of a nuclear signal motif by monoubiquitination leads to mislocalization and degradation of the regulatory enzyme cytidylyltransferase. *Mol Cell Biol*. 2009;29(11):3062–3075.
63. D'Aiuto L, et al. Generation of three-dimensional human neuronal cultures: application to modeling CNS viral infections. *Stem Cell Res Ther*. 2018;9(1):134.
64. Bateman NW, Sun M, Hood BL, Flint MS, Conrads TP. Defining central themes in breast cancer biology by differential proteomics: conserved regulation of cell spreading and focal adhesion kinase. *J Proteome Res*. 2010;9(10):5311–5324.
65. McQuin C, et al. CellProfiler 3.0: Next-generation image processing for biology. *PLoS Biol*. 2018;16(7):e2005970.
66. Mallampalli RK, Ryan AJ, Salome RG, Jackowski S. Tumor necrosis factor-alpha inhibits expression of CTP:phosphocholine cytidylyltransferase. *J Biol Chem*. 2000;275(13):9699–9708.
67. Chen BB, Coon TA, Glasser JR, Mallampalli RK. Calmodulin antagonizes a calcium-activated SCF ubiquitin E3 ligase subunit, FBXL2, to regulate surfactant homeostasis. *Mol Cell Biol*. 2011;31(9):1905–1920.